Lorentz force velocimetry using a bulk HTS magnet system: proof-of-concept

OPEN ACCESS
IOP Publishing
Superconductor Science and Technology
Supercond. Sci. Technol. **31** (2018) 084003 (9pp)
https://doi.org/10.1088/1361-6668/aac949

Lorentz force velocimetry using a bulk HTS magnet system: proof-of-concept

O V Vakaliuk[1], M D Ainslie[2] and B Halbedel[1]

[1] Group for Inorganic-Nonmetallic Materials, Institute for Material Engineering and Institute for Micro- and Nanotechnologies, Technische Universität Ilmenau, Gustav-Kirchhoff-Str. 6, D-98693, Ilmenau, Germany
[2] Bulk Superconductivity Group, Department of Engineering, University of Cambridge, Trumpington Street, Cambridge, CB2 1PZ, United Kingdom

E-mail: oleksii.vakaliuk@tu-ilmenau.de

Received 30 March 2018, revised 21 May 2018
Accepted for publication 31 May 2018
Published 25 June 2018

Abstract

This paper presents a proof-of-concept of the idea of using bulk high-temperature superconducting (HTS) materials as quasi-permanent magnets that would form, in the future, an integral part of an advanced Lorentz force velocimetry (LFV) system. The experiments, calculations and numerical simulations are performed in accordance with the fundamental theory of LFV, whereby a moving metal rod passes through a static magnetic field, in our case generated by the bulk HTSs. The bulk HTS magnet system (MS) consists of two Y–Ba–Cu–O samples in the form of bulk cylindrical discs, which are encapsulated in an aluminium holder and wrapped with styrofoam. The aluminium holder is designed to locate the bulk HTS magnets on either side of the metal rod. After field cooling magnetisation with an applied field of 1.5 T at 77 K, the bulk HTS MS provides a quasi-permanent magnetic field over 240 s, enabling Lorentz force measurements to be carried out with a constant velocity of the metal rod. Two sets of Lorentz force measurements with copper and aluminium rods with velocities ranging from approximately 54–81 mm s^{-1} were performed. The obtained results, which are validated using a numerical model developed in COMSOL Multiphysics, demonstrate the linear relationship between the Lorentz force and velocity of the moving conductor. Finally, the potential of generating very high magnetic fields using bulk HTS that would enable LFV in even weakly-conducting and slow-flowing fluids, e.g., glass melts, is discussed.

Keywords: Lorentz force velocimetry, bulk high-temperature superconductors, flow rate measurement, glass melts, trapped field magnets, numerical simulation, finite-element method

(Some figures may appear in colour only in the online journal)

1. Introduction

Velocity or flow rate measurement of fluids is of great importance to industry because it improves the reliability of accounting and facilitates stricter control of production processes. In particular, there is a growing need for non-invasive measurements, in view of the hygienic requirements in the pharmaceutical and food industries [1]. Furthermore, there is a demand for a non-contact measurement method in several other industrial sectors (see table 1):

(i) liquid metals for high-quality aluminium, cooper and steel production [2];
(ii) glass melts for the manufacturing of high-quality glass products [3, 4];
(iii) molten salt energy or storage systems [5].

Currently-used flow measurement techniques (e.g. magneto-inductive) require an electrical contact to the wall of the channel directly to the fluid [6, 7], or when using optical

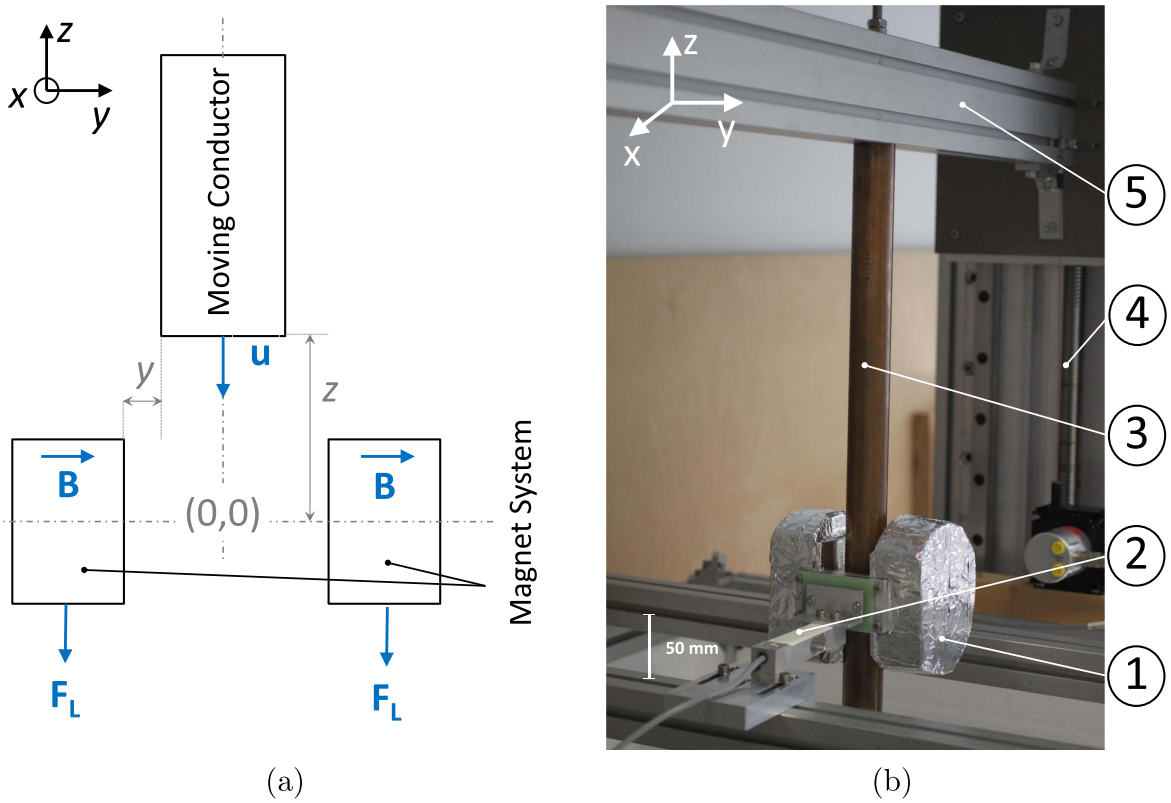

Figure 1. (a) Schematic of the LFV proof-of-concept. (b) Photograph of the realised LFV experimental setup, which consists of five main components: (1) HTS magnet system, (2) force sensor, (3) metal rod, (4) linear drive and (5) aluminium rack.

Table 1. Classification of aggressive and opaque fluids with respect to the measurement forces resulting from equation (1) (with $B = 0.1$ T and $V = 10^{-3}$ m^3).

Industrial sector	Fluid type	σ (S m^{-1})	u (m s^{-1})	F_L (N)
Material inspection	Solid metal	10^7	1	10^2
Metallurgy	Liquid metal	10^6	1	10^1
Chemistry	Acid, base	10^2	1	10^{-3}
Glass/semiconductor	Glass melts	10^1	10^{-2}	10^{-6}
Pharmacy/food	Ultra pure water	10^{-6}	1	10^{-11}

methods, the wall should be transparent. In addition, the fluid itself can impose limitations, especially when it is opaque, hot or chemically aggressive.

To overcome this limitation, Lorentz force velocimetry (LFV) has been introduced and studied in recent years, extensively in the pursuit of the non-invasive measurements of the velocity or flow rate in opaque and aggressive fluids [2, 8–14]. The LFV working principle relies on measuring the force, namely the Lorentz force, that is generated by the relative motion of an electrically conductive medium through a transversely applied magnetic field. The theory of LFV was introduced in [8] and expressed through the scaling law:

$$F_L \sim \sigma \cdot u \cdot B^2 \cdot V \tag{1}$$

where the Lorentz force F_L depends linearly on electrical conductivity σ, mean flow velocity u, magnetic flux density B and a characteristic volume V. By measuring the resultant reaction force for a prescribed magnetic flux density and known electrical conductivity, it is possible to estimate the mean flow velocity of the fluid. It should be stressed that equation (1) holds for stationary flow or for the steady state motion of a solid conductor of a constant cross-section [8, 9, 15]. Figure 1(a) illustrates the LFV principle: the primary magnetic field (shown by the B) is generated by a magnet system and when the moving conductor passes through this magnet system, the interaction between induced eddy currents and the primary magnetic field causes a retarding force to act on the moving conductor [8]. In accordance with Newton's third law, a force (shown by the $\boldsymbol{F_L}$ vector) with a magnitude equal to the retarding force, but in the opposite direction, acts on the magnet system along the moving direction.

It has been shown that LFV works well for liquid metals due to their relatively high electrical conductance ($\sigma \sim 10^6$ S m^{-1}) [2, 9, 10]. However, in case of weakly-conducting and slow-flowing fluids, LFV treats the measurement of tiny forces down to 10 nN, depending on the fluid velocity and electrical conductivity (see table 1). The experimental

investigation of LFV for salted water (as a model fluid) of varying electrical conductivity and flow velocity was reported in several past works [11–14]. This was realised by employing a high-precision force measurement system (FMS), i.e. electromagnetic force compensated weighing cell (Sartorius Lab Instruments), in a combination with an optimised Halbach array of permanent magnets (PMs) [16] of 1 kg. The PMs were placed at the minimum distance from the flowing salted water, thereby providing effective interaction of the magnetic flux density with the flow volume. However, in the case of aggressive fluids (i.e. glass melts) the realization of close magnetic interaction with the fluid is not possible due to the large isolation walls. Furthermore, the surface magnetic flux density of the strongest available NdFeB PMs is limited to about 0.5 T [17].

Hence, even in early works on LFV [11–14, 18], the prospective idea to employ bulk HTS magnets has been proposed, because of their ability to act as much stronger trapped field magnets. Record trapped fields over 17 T using field cooling (FC) magnetisation was achieved in [19, 20], whilst a maximum trapped field over 5 T was reported in [21] using compact and fast pulsed field magnetisation. Furthermore, bulk HTS magnets continue to be investigated as a replacement for conventional PMs in a variety of applications [22–34].

In contrast to PMs, the bulk HTS magnet has a characteristic feature of generating a conically-shaped trapped magnetic flux density, B_T, distribution, that has a sharp field gradient [35]. Whether this feature adequately replicates the LFV theory [8] (the linear relationship between F_L and the product $\sigma \cdot u \cdot B^2$ in equation (1)) is one question to be addressed by current experimental efforts. Hence, the main objective of this study is to examine the feasibility of bulk HTS magnets as a substitute for existing NdFeB PMs in LFV.

The paper is organized as follows: section 2 presents the experimental setup, including the FMS and the design of the bulk HTS MS. This includes the method of cooling and magnetising the bulks as trapped field magnets, as well as the magnetic field distribution from the magnets. In particular, section 2.4 gives details on the Lorentz force measurements. A numerical model in COMSOL Multiphysics is then introduced in section 3 to validate the experimental results and the theory of LFV as applied to this system. Finally, section 4 discusses the obtained experimental results and ends with a view to further developing the system practically in section 5.

2. Experimental

2.1. Overview

The experiments were carried out using a 'dry calibration' setup [10, 36], developed at the Department of Engineering, Techniche Universität Ilmenau, but upgraded with the bulk HTS MS and an appropriate load cell for the force measurements. The idea of the 'dry calibration' implies the replacement of a fluid flow with the controlled motion of a solid conductor (e.g. metal rod) of a fixed geometry [10]. This enables a fairly straightforward way of carrying out fundamental LFV measurements.

2.2. Experimental set up

Figure 1 shows a schematic diagram and photograph of the experimental setup used to test LFV using the bulk HTS MS. The setup consists of five main components: (1) bulk HTS MS, (2) load cell, (3) metal rod, (4) linear drive and (5) aluminium rack. The experimental procedure is fully automated: an IBA-Automation environment controls the linear drive and is used for data acquisition [37]. The linear drive executes a repetitive motion of the metal rod with a prescribed constant velocity. At first, it moves downwards, then reverses its direction and moves back to its initial position. The cylindrical long metal rods have a length of 1000 mm and a diameter of 40 mm. Two types of metal rods were used: copper with an electrical conductivity of $\sigma_{Cu} = 58.96 \pm 0.20\,\mathrm{MS\,m^{-1}}$ and aluminium alloy (AlMgSi) with $\sigma_{Al} = 19.43 \pm 0.03\,\mathrm{MS\,m^{-1}}$ [37]. The mean velocities of the copper rod were $u = [54;\ 64;\ 76;\ 81]\ \mathrm{mm\,s^{-1}}$. For the aluminium rod, F_L measurements with only two velocities of $u = [70;\ 81]\ \mathrm{mm\,s^{-1}}$ were possible, due to its lower conductivity and limitations related to the resolution of the present LFV measurement system. Note, the metal rod starts its motion being $z = +165$ mm distant from the centre of the bulk HTS MS, whilst the distances between the surfaces of the bulk HTS and the metal rod is $y = +12$ mm on both sides, as shown in figure 1(a).

A commercial load cell (Model PW6D, Hottinger Baldwin Messtechnik GmbH) combined with an analogue measuring amplifier (SOEMER Messtechnik GmbH) was used for the force measurements. The force is measured in terms of a voltage with the accuracy class C3. *In-situ* force–voltage calibration was performed using E2 class certified calibration masses of 5, 10, 20 and 100 g. Details on the force measurement calibration are provided in appendix A1.

2.3. Bulk high-temperature superconducting magnet system

The bulk HTS MS consists of two Y–Ba–Cu–O samples in the form of a cylindrical disc with a diameter of 46 mm and a thickness of 16 mm, provided by Adelwitz Technologiezentrum GmbH. The Y–Ba–Cu–O bulks were encapsulated in an aluminium holder and arranged opposite each other with a distance of 64 mm between. The aluminium holders were wrapped in styrofoam and radiation shielding tape, in order to reduce warming to room temperature. A G-10 plate of thickness of 10 mm was used to prevent heat transfer from the HTS MS to the load cell.

The bulk HTS MS must be magnetised before coupling with the force sensor. The magnetisation was carried out in the room temperature bore of a superconducting solenoid magnet (Cryogenics Ltd., London, UK) using FC magnetisation: at first, an applied field of $B_A = 1.5$ T was generated; then, the bulk HTS MS was cooled down to 77 K. Cooling was achieved by immersing the entire HTS MS in an open styrofoam container with liquid nitrogen (LN_2), which was

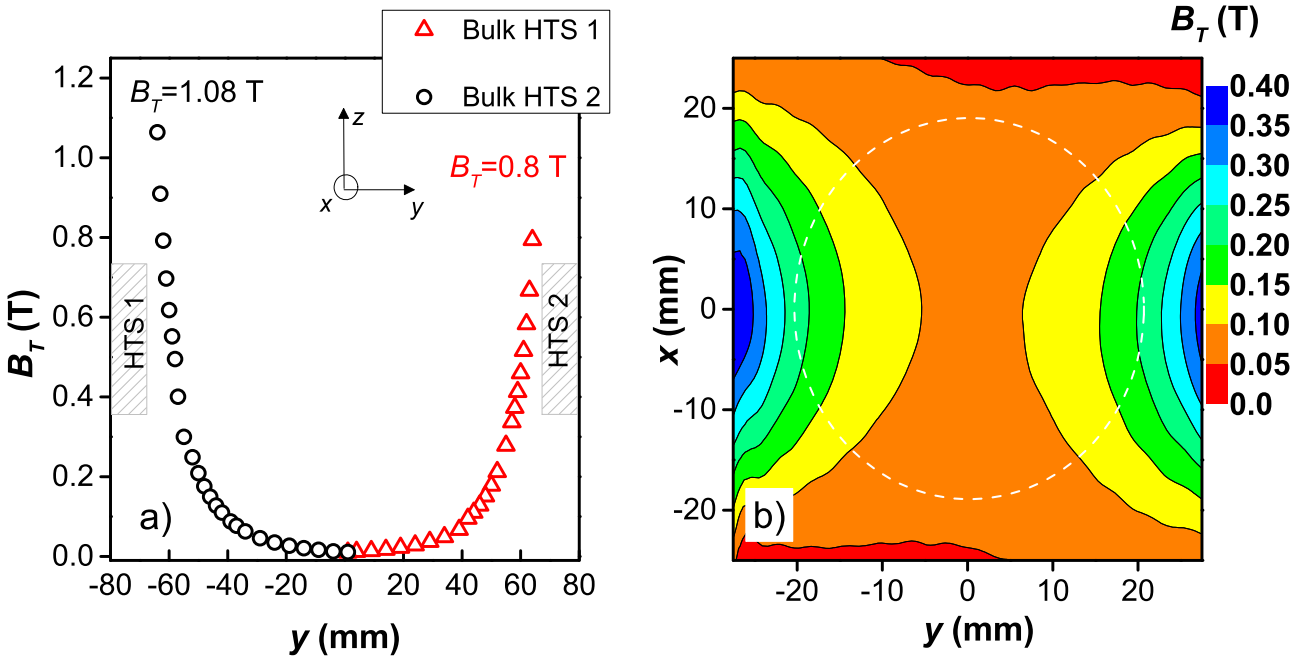

Figure 2. (a) The peak trapped magnetic flux density $B_T(y)$ for each bulk HTS as a function of distance (along the y-axis) with a maximum field of 1.08 T (left) and 0.8 T (right) at the bulk surfaces. The shaded rectangles indicate the HTS bulks (left and right). (b) The magnetic flux density distribution $B_T(x, y)$ in the bulk HTS MS gap. The drawn circle indicates the location of the metal rod. Firstly, this was measured for each bulk HTS separately, then for the gap between the two bulks in the HTS MS.

refilled periodically, due to the evaporation of LN_2. Afterwards, B_A was ramped down at a ramp rate of 0.092 T min^{-1}. A certain magnetic flux density B_T can be retained in the bulks, because of the trapped flux and resultant induced superconducting current. When B_A reduced to zero, the B_T (hereafter B_T indicates the B_y-component of B) distribution was measured using a scanning Hall probe arrangement to characterise the bulk HTS.

At first, B_T was measured for each bulk HTS separately, then for the gap between the two magnetised bulks in the HTS MS. The peak trapped magnetic flux density $B_T(y)$ for each bulk HTS as a function of distance (along the y-axis) is shown in figure 2(a). A maximum field of 1.08 T (left) and 0.8 T (right) at the bulk surfaces was recorded for each bulk HTS, respectively. The magnetic flux distribution $B_T(x, y)$ in the gap of the bulk HTS MS is presented in figure 2(b). It is qualitatively consistent with data reported in [24, 38–40], where a similar bulk HTS face-to-face arrangement was employed. The relatively large gap between the bulk HTSs in this study was required to enable the unobstructed motion of the metal rod through the bulk HTS MS (see figure 1). In future studies, this gap should be minimised for the proper utilisation of the magnetic field, since the maximum trapped magnetic flux density exponentially decreases with increasing distance (see figure 2(a)). To achieve this, a novel cooling system for the bulk HTS MS must be developed.

2.4. Lorentz force measurements

When the bulk HTS MS is coupled with the load cell and mounted to the LFV setup, continuous cooling in a LN_2 bath is not possible, because of the mass and volume restriction of the load cell. Hence, it was necessary during the force measurements to extract the bulk HTS MS from its LN_2 bath. The bulk HTS MS holds a trapped field for a specific period of time until it begins to warm up to room temperature, during which LFV measurements for one assigned velocity are performed. In addition, the temperature of the system during LFV measurements was monitored with a Cernox sensor.

An example of the periodic rod motion $L(t)$ for a velocity of $u = 54$ mm s^{-1} and the corresponding time sequence of the Lorentz force measurements is depicted in figure 3(a). The experimental procedure is as follows:

(i) [$t_0 = 0$; $t_1 = 5$ s]—extraction of the magnetised bulk HTS MS from the LN_2 bath;
(ii) [$t_1 = 5$; $t_2 = 23$ s]—coupling with the force sensor and beginning motion of the rod;
(iii) [$t_2 = 23$; $t_3 = 500$ s]—Lorentz force measurements;
(iv) [$t_3 = 500$ s]—stopping the rod motion and decoupling of the bulk HTS MS.

In the future, a more practical design of the bulk HTS MS with robust and long-term operation is required at temperatures $T < 77$ K, hence cryogenic refrigeration in a compact and light-weight cryostat is an issue to be resolved.

Figure 3(b) shows the time dependent data for $B_T(t)$ and $T(t)$ (see the arrow, different scales are used) in the gap of the MS in the vicinity ($y \approx 25$ mm, equivalent to 7 mm from the bulk surface) of the one bulk HTS. $B_T(t)$ remains almost constant up to 240 s, and then gradually reduces to zero due to warming at room temperature and flux creep [41]. Although the direct temperature measurement of the bulk HTS during the $F_L(t)$ experiments was not performed, its influence on the HTS bulks is indirectly included in the measured $B_T(t)$

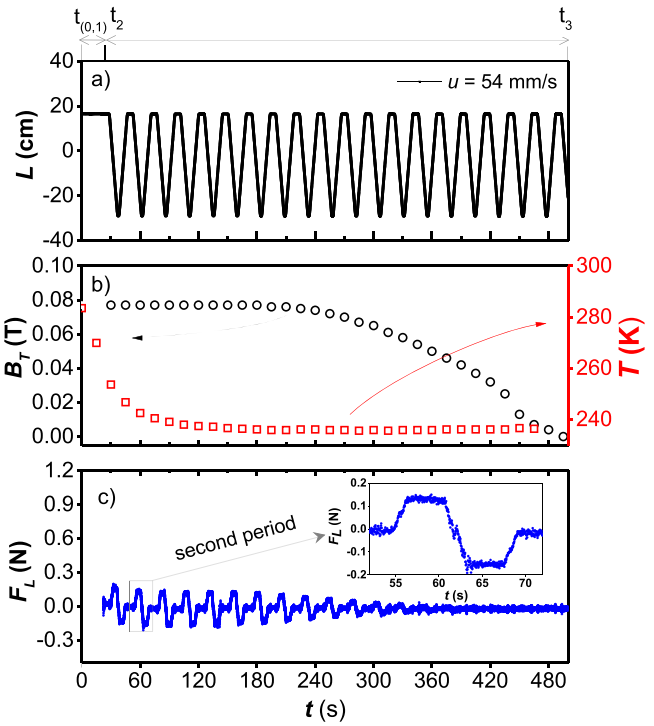

Figure 3. (a) An example of the periodic rod motion $L(t)$ with a velocity of $u = 54$ mm s^{-1}. The time sequence of the experiments is indicated as follows: [$t_0 = 0$; $t_1 = 5$ s]—extraction of the bulk HTS MS from the LN_2 bath; [$t_1 = 5$; $t_2 = 23$ s]—coupling with the force sensor and beginning the motion of the rod; [$t_2 = 23$; $t_3 = 500$ s]—LFV measurements, [$t_3 = 500$ s]—stopping the rod motion and decoupling of the bulk HTS MS. (b) Trapped field B_T at a distance of 7 mm from the surface of one HTS bulk as function of time t. The field was recorded by a Hall probe right after the HTS magnet system was removed from the LN_2 container. In addition, the time dependent temperature behaviour of the load cell $T(t)$ (see the arrow, different scales are used) is included. (c) The Lorentz force F_L as a function of time t which acts on HTS MS upon repetitive movement of the metal rod. Inset: measured data for $F(t)$ for the second period.

dependence. Still, in order to obtain a correct force signal, the temperature of the load cell was measured: $T(t)$ drops at the beginning from room temperature down to 240 K and remains constant.

Figure 3(c) shows an example of the measured Lorentz force $F_L(t)$ for the prescribed velocity of 54 mm s^{-1}. $F_L(t)$ exhibits a periodic step function behaviour with the anticipated attenuation due to the above effects. At the beginning, a steep decrease in the amplitude of $F_L(t)$ is attributed to the temperature drop, while gradual attenuation is consistent with the change in $B_T(t)$. Obtaining experimental data under the conditions of constant $B_T(t)$ and $T(t)$ is important, since any changes strongly influence the F_L measurements [14]. Therefore, the estimation of the Lorentz force was calculated for the second period of metal rod motion (see figure 3(c) and its inset), where $B_T(t)$ and $T(t)$ are nearly constant.

The detailed $F_L(t)$ response of the metal rod for the second period is presented in the inset of figure 3(c). Initially, the force is zero, when the metal rod is not moving. Then the metal rod approaches the bulk HTS MS resulting in an increase in F_L. Stationary motion of the metal rod through the bulk HTS MS results in a plateau-like $F_L(t)$. Afterwards, the metal rod reverses the direction, yielding an analogous but negative force. Admittedly, some asymmetry between the positive and negative force signals arises because of asymmetric up- and down-movement (i.e. along z-axis) and off-axis alignment (i.e. along x-axis and/or y-axis), as was stressed in [15].

3. Numerical model

Numerical modelling is a powerful tool to validate and interpret experimental results and is useful for predicting the performance of bulk superconductors in practical applications [42]. To validate the experimental results in this work, a fully 3D model based on the finite-element method was implemented using the AC/DC module of COMSOL Multiphysics 5.3a. The geometry of the model is shown in figure 3, with the same dimensions as the experimental setup described in section 2. The electromagnetic properties of the bulk HTS magnets and the metal rod are implemented using the AC/DC module's magnetic and electric fields interface, satisfying Ampere's law:

$$\nabla \times \boldsymbol{H} = \boldsymbol{J} \tag{2}$$

and current conservation, such that

$$\nabla \cdot \boldsymbol{J} = 0. \tag{3}$$

The bulk HTS magnets are assumed to be fully magnetised, utilising the 'external current density' node to assume a current density of constant J_c [43]. The value of J_c for each magnet is determined from the experimental trapped field measurements of the bulks (see figure 2(a)), where $B_{T,1} = 1.08$ T and $B_{T,2} = 0.8$ T, and the following equation based on the critical state model presented by Bean [35, 44] and application of the Biot–Savart law [43]:

$$B_T = k\mu_0 J_c a, \tag{4}$$

where B_T is the peak trapped magnetic flux density at the centre of the top surface of a c-axis oriented, single-grain bulk superconductor, μ_0 is the permeability of free space, J_c is the critical current density of the superconducting material, and a is the sample radius. k is the correction factor to the simple Bean (slab) approximation due to the finite thickness, t, of a disc-shaped bulk superconductor:

$$k = \frac{t}{2a}\ln\left(\frac{a}{t} + \sqrt{1 + \left(\frac{a}{t}\right)^2}\right). \tag{5}$$

This results in an average, in-field J_c for the two bulks of $J_{c,1} = 9.9 \times 10^7$ A m^{-2} and $J_{c,2} = 7.33 \times 10^7$ A m^{-2}. The resultant magnetic flux density within the rod cross-section across the centre of the bulk HTS MS is shown in figure 4(b). The calculated magnetic flux density is consistent with the experimental results shown in figure 2(b).

The movement of the metal rod through the magnets is simulated by applying a velocity (Lorentz term) condition to

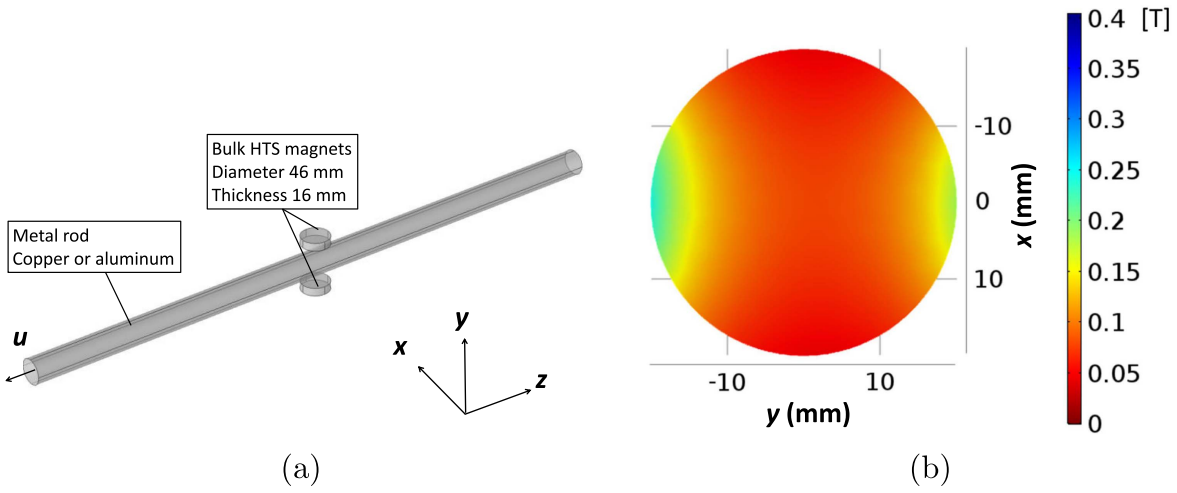

Figure 4. (a) Fully 3D model for the numerical simulation of the fundamental LFV proof-of-concept. The bulk HTS magnets are assumed to be fully magnetised, carrying a constant J_c corresponding to the trapped field measurements of each bulk (see figure 2(a)). The movement of the metal rod through the magnets is simulated by applying a velocity (Lorentz term) to the rod sub-domain. (b) Magnetic flux density within the rod cross-section aligned with the centre of the bulk HTS MS. The calculated magnetic flux density is consistent with the experimental results shown in figure 2(b).

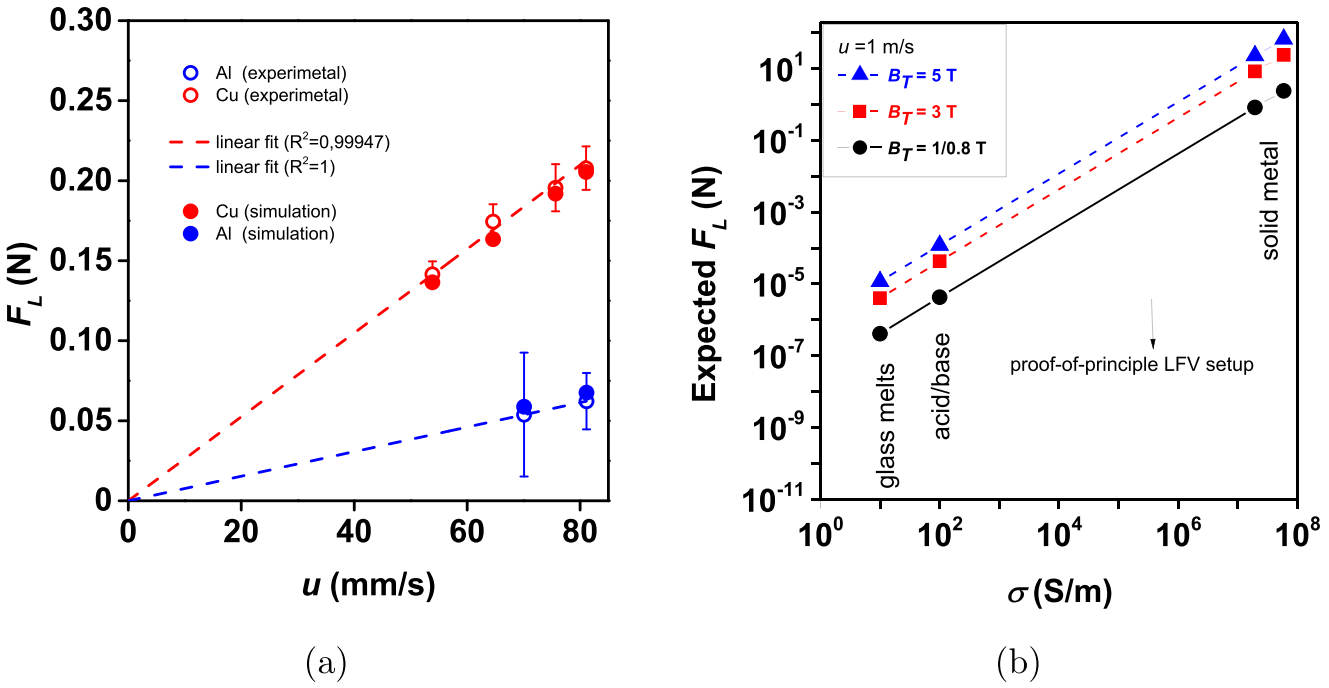

Figure 5. (a) Lorentz force F_L as function of a velocity u for the copper and aluminium rods. Open circles indicate the experimental results, and the solid circles indicate the simulation results. The dashed lines indicate the linear fit to the experimental results. (b) Expected Lorentz forces as function of electrical conductivity for relevant fluids, e.g. solid metals, acids/base and glass melts, including the experimental results presented in this paper.

the metal rod sub-domain in COMSOL, such that

$$\boldsymbol{J} = \sigma(\boldsymbol{E} + \boldsymbol{u} \times \boldsymbol{B}). \tag{6}$$

Finally, the force is calculated by

$$\boldsymbol{F} = \int_V F_z \cdot dV = \int_V (B_y J_x - B_x J_y) \cdot dV. \tag{7}$$

The calculated force for the two rods for different rod velocities is compared with the experiments in the following section (see figure 5(a)).

4. Results and discussion

With the aim of scaling the force and velocity according to equation (1), a set of LFV measurements with prescribed mean velocities u were carried out. In the case of the copper rod, u = [54; 64; 76; 81] mm s^{-1}, while for the aluminium rod: u = [70; 81] mm s^{-1}. The results of the Lorentz force measurements obtained experimentally with those calculated numerically are plotted against the velocity for the aluminium and copper rods in figure 5(a). F_L is linearly dependent on the

velocity and the electrical conductivity of the moving metal rods, which is consistent with theory (see equation (1)) [8]. Additionally, the F_L values obtained with same-sized copper and aluminium rods for one prescribed velocity, e.g. $u = 81$ mm s^{-1}, scales as σ_{Cu}/σ_{Al}. Unfortunately, in the case of aluminium, the induced Lorentz force approaches the resolution limit of the current LFV setup and therefore can result in significant measurement errors.

Furthermore, it is shown that the experimental and simulation results agree well, validating the numerical model (time independent, 3D) as a fast and accurate tool to predict the LFV performance. Thus, the expected F_L with respect to the electrical conductivity of relevant fluids, e.g. solid metals, acids/base and glass melts (see table 1), can be estimated in accordance with equation (1). It should be noted that the F_L values are valid only for our particular design of the proof-of-principle LFV setup (see figure 1(b)) and may vary for each individual system differently: in particular, the spatial distribution of the magnetic flux density within the interaction volume of the moving conductor. Figure 5(b) shows the expected F_L as a function of the electrical conductivity. With use of the present proof-of-principle LFV setup (the bulk HTS trap $B_T = 0.94$ T, i.e., the average of 1.08/0.8 T), the generated forces for weakly-conducting and slow-flowing fluids are in the range of μN and below. In particular, $F_L \sim 10^{-6}$ N for acids/bases and $F_L \sim 10^{-7}$ N for glass melts. It is immediately clear that the use of the bulk HTS MS with higher trapped fields of 3 and 5 T enhance the resultant F_L over an order of magnitude and thereby the F_L-resolution. This provides evidence that the bulk HTS MS is feasible and serves as a starting point for the future development of a new LFV prototype with improved performance.

Still, for practical LFV application to weakly-conducting and slow-flowing fluids, a high-precision force measurement in combination with the bulk HTS magnets is required. Measurements of such forces can be achieved by replacing the simplified load cell with a torsion balance based system for high-precision force measurement (TFMS), proposed in [45, 46]. In order to raise the issue of the limiting total mass (which is always an issue for high-precision force measurements), the bulk HTS MS and TFMS can be merged within an integrated cryostat. This idea was patented by the authors [47] and the relevant portable LFV prototype is currently under construction.

5. Conclusions

The current work demonstrates the applicability of a bulk HTS magnet system (MS) to Lorentz force velocimetry (LFV) using an experimental setup, where the Lorentz force, acting on the moving metal rod, is measured by a load cell that carries the bulk HTS MS. The bulk HTS MS offers higher magnetic field than the previously used NdFeB PM-based system, with a similar mass, despite it requiring appropriate cooling and magnetisation. However, the magnetic field of the bulk HTS magnets strongly decreases with a distance, implying that proximity of the bulk HTS MS to the moving metal rod is important for optimal LFV performance.

The obtained experimental and numerical simulation results agree well, exhibiting the linear relationship between the Lorentz force and product of the electrical conductivity and velocity, in accordance with LFV theory [8]. Hence, these results serve as a starting point for the future development of a new LFV prototype with improved performance.

In particular, the LFV prototype currently under construction consists of bulk HTS magnets that are combined with the high-precision TFMS and encapsulated in an integrated cryostat. All these features enable a further extension of the LFV application to a number of industrial weakly-conducting and slow-flowing fluids, e.g. glass, molten salts melts and/or acid and lyes.

Finally, a simple, time independent 3D numerical model has been developed as a fast and accurate tool to predict the LFV performance, but a time dependent, dynamic model should be developed in the future that can consider more detailed superconducting properties, including different magnetisation process and flux creep effects.

Acknowledgments

The authors MSc Oleksii Vakaliuk and Dr Bernd Halbedel acknowledge the German Research Foundation (DFG) within the Research Training Group Lorentz Force Velocimetry and Lorentz Force Eddy Current Testing (RTG-1567/3) for the financial support. The authors also thank M Weidner for supporting draft of the proof-of-principle concept and A Thieme for providing force measurements equipment. Assistance of L Kellmann and G Langrof during the experiments is appreciated. Dr Mark Ainslie would like to acknowledge the support of an Engineering and Physical Sciences Research Council (EPSRC) Early Career Fellowship EP/P020313/1. Additional data related to this publication are available at the University of Cambridge data repository (https://doi.org/10.17863/CAM.21587).

Appendix. Force–voltage calibration of the load cell

Masses of 5, 10, 20 and 100 g (KERN & SOHN GmbH) were used to generate a force on the load cell (Model PW6D, Hottinger Baldwin Messtechnik GmbH) in order to calibrate the output voltage signal from the measuring amplifier directly into a force. The measured calibration curve $U(F)$ and its linear fit with a regression coefficient $R^2 = 0.999\,96$ is shown in figure A1.

The uncertainty for the obtained force data ΔF was computed on the basis of the measured standard deviation ΔU of the voltage recorded by the the IBA-Automation environment [37] and uncertainty of the E2 class certified

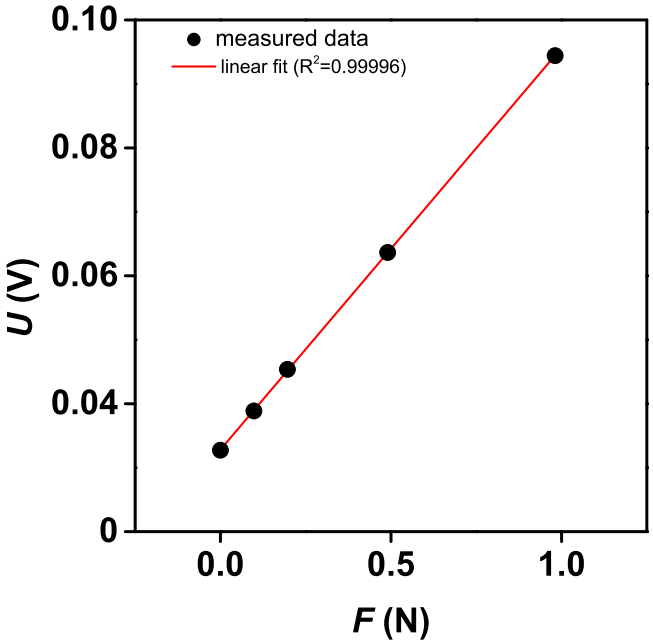

Figure A1. The measured calibration curve $U(F)$ and its linear fit with a regression coefficient $R^2 = 0.999\,96$.

calibration masses using:

$$\frac{\Delta F}{F} = \sqrt{\left(\frac{\Delta U}{U}\right)^2 + \left(\frac{\Delta m}{m}\right)^2}, \qquad \text{(A.1)}$$

where ΔU and Δm are the measured uncertainty of the voltage U and mass m, respectively.

ORCID iDs

O V Vakaliuk https://orcid.org/0000-0002-0813-1078
M D Ainslie https://orcid.org/0000-0003-0466-3680
B Halbedel https://orcid.org/0000-0002-7181-1359

References

[1] Prabu S L and Suriyaprakash T N K 2010 Cleaning validation and its importance in pharmaceutical industry *Pharma Times* **42** (7)
[2] Kolesnikov Y, Karcher C and Thess A 2011 Lorentz force flowmeter for liquid aluminum: laboratory experiments and plant tests *Metall. Mater. Trans.* B **42** 441–50
[3] Mauro J and Zanotto E 2014 Two centuries of glass research: historical trends, current status, and grand challenges for the future *Int. J. Appl. Glass Sci.* **5** 313–27
[4] Torres-Perez J O 2016 Nutzung von Lorentzkräften für Mischprozesse in der Chemie- und Glasindustrie *PhD Thesis* Technische Universität Ilmenau
[5] Herrmann U, Kelly B U and Price H 2004 Two-tank molten salt storage for parabolic trough solar power plants *Energy* **29** 883–93
[6] Buchenau D 2012 Entwicklung von kontaktlosen und zeitlich hochauflösenden Strömungs- und Durchflusssensoren für Flüssigmetallströmungen *PhD Thesis* Karlsruher Instituts fuer Technologie (KIT)
[7] Wegfrass A 2013 Experimentelle Untersuchungen zur Anwendbarkeit der LKA auf schwach leitfähige Fluide *PhD Thesis* Technische Universität Ilmenau
[8] Thess A, Votyakov E and Kolesnikov Y 2006 Lorentz force velocimetry *Phys. Rev. Lett.* **96** 164501
[9] Thess A, Votyakov E and Kolesnikov Y 2007 Theory of the Lorentz force flow meter *New J. Phys.* **9** 299
[10] Minchenya V, Karcher C, Kolesnikov Y and Thess A 2011 Calibration of the Lorentz force flowmeter *Flow Meas. Instrum.* **22** 242–7
[11] Wegfrass A, Diethold C, Werner M, Resagk C, Fröhlich T, Halbedel B and Thess A 2012 Flow rate measurement of weakly conducting fluids using Lorentz force velocimetry *Meas. Sci. Technol.* **23** 105307
[12] Wegfrass A, Diethold C, Werner M, Fröhlich T, Halbedel B, Hilbrunner F, Resagk C and Thess A 2012 A universal noncontact flowmeter for liquids *Appl. Phys. Lett.* **100** 194103
[13] Halbedel B, Resagk C, Wegfrass A, Diethold C, Werner M, Hilbrunner F and Thess A 2013 A novel contactless flow rate measurement device for weakly conducting fluids based on Lorentz force velocimetry *Flow, Turbul. Combust.* **92** 361–9
[14] Vasilyan S, Ebert R, Weidner M, Rivero M, Halbedel B, Resagk C and Fröhlich T 2015 Towards metering tap water by Lorentz force velocimetry *Meas. Sci. Technol.* **26** 115302
[15] Alferenok A, Pothrat A and Lüdtke U 2013 Optimal magnet configurations for Lorentz force velocimetry in low conductivity fluids *Meas. Sci. Technol.* **24** 065303
[16] Werner M and Halbedel B 2012 Optimization of NdFeB magnet arrays for improvement of Lorentz Force Velocimetry *IEEE Trans. Magn.* **48** 2925–8
[17] Gutfleisch O, Willard M, Ekkes B, Brck E E, Chen C, Sankar S and Liu Ping J 2011 Magnetic materials and devices for the XXI century: stronger, lighter, and more energy efficient *Adv. Mater.* **23** 821–42
[18] Ebert R, Leineweber J and Resagk C 2015 Performance enhancement of a Lorentz force velocimeter using a buoyancy-compensated magnet system *Meas. Sci. Technol.* **26** 075301
[19] Tomita M and Murakami M 2003 High-temperature superconductor bulk magnets that can trap magnetic fields of over 17 Tesla at 29 Kelvin *Nature* **421** 517
[20] Durrell J H *et al* 2014 A trapped field of 17.6 T in melt-processed, bulk Gd–Ba–Cu–O reinforced with shrink-fit steel *Supercond. Sci. Technol.* **27** 082001
[21] Fujishiro H, Tateiwa T, Fujiwara A, Oka T and Hayashi H 2006 Higher trapped field over 5 T on HTSC bulk by modified pulse field magnetizing *Proc. 18th Int. Symp. on Superconductivity (ISS 2005); Physica* C **445–448** 334–8
[22] Hull J R and Murakami M 2004 Applications of bulk high-temperature superconductors *Proc. IEEE* **92** 1705–18
[23] Oka T, Kanayama H, Fukui S, Ogawa J, Sato T, Ooizumi M, Terasawa T, Itoh Y and Yabuno R 2008 Application of HTS bulk magnet system to the magnetic separation techniques for water purification *Physica* C **468** 2128–32
[24] Oka T, Kanayama H, Tanaka K, Fukui S, Ogawa J, Sato T, Yamaguchi M, Ooizumi M, Yokoyama K and Noto K 2009 Study on magnetic separation system using high T_c superconducting bulk magnets for water purification technique *J. Phys.: Conf. Ser.* **156** 012031
[25] Hirota Y, Akiyama Y, Izumi Y and Nishijima S 2009 Fundamental study for development magnetic drug delivery system *Proc. 21st Int. Symp. on Superconductivity (ISS 2008); Physica* C **469** 1853–6
[26] Ohsaki H, Terao Y and Sekino M 2010 Wind turbine generators using superconducting coils and bulks *J. Phys.: Conf. Ser.* **234** 032043

[27] Ogawa K, Nakamura T, Terada Y, Kose K and Haishi T 2011 Development of a magnetic resonance microscope using a high T_c bulk superconducting magnet *Appl. Phys. Lett.* **98** 234101

[28] Mishima F, Terada T, Akiyama Y and Nishijima S 2011 High gradient superconducting magnetic separation for iron removal from the glass polishing waste *IEEE Trans. Appl. Supercond.* **21** 2059–62

[29] Nakamura T, Itoh Y, Yoshikawa M, Oka T and Uzawa J 2007 Development of a superconducting magnet for nuclear magnetic resonance using bulk high-temperature superconducting materials *Concepts Magn. Reson.* B **31B** 65–70

[30] Yanamoto T, Izumi M, Yokoyama M and Umemoto K 2015 Electric propulsion motor development for commercial ships in Japan *Proc. IEEE* **103** 2333–43

[31] Werfel F N, Floegel-Delor U, Riedel T, Rothfeld R, Schirrmeister P, Wippich D and Koenig R 2015 Technical progress in HTS magnetic bulk application development *IEEE Trans. Appl. Supercond.* **25** 3600304

[32] Werfel F N, Floegel-Delor U, Rothfeld R, Riedel T, Schirrmeister P and Koenig R 2016 Experiments of superconducting maglev ground transportation *IEEE Trans. Appl. Supercond.* **26** 3602105

[33] Oka T, Takayanagi Y, Machida S, Ichiju K, Fukui S, Ogawa J, Sato T, Ooizumi M, Tsujimura M and Yokoyama K 2016 Magnetic separation for recovering Ni compounds from plating waste with use of HTS bulk magnets *IEEE Trans. Appl. Supercond.* **26** 3700204

[34] Werfel F N, Floegel-Delor U, Rothfeld R, Riedel T, Schirrmeister P, Koenig R and Kantarbar V 2017 Impact of cryogenics and superconducting components for HTS magnetic levitation devices *IEEE Trans. Appl. Supercond.* **27** 3600905

[35] Bean C P 1962 Magnetization of hard superconductors *Phys. Rev. Lett.* **8** 250–3

[36] Weidermann C, Sokolov I and Thess A 2014 Lorentz force and joule heat induced in an electrically conducting plate moving with time-dependent velocity under the influence of a homogeneous magnetic field *IEEE Trans. Magn.* **50** 7027209

[37] Weidermann C 2013 Design and laboratory test of a Lorentz force flowmeter for pipe flows *PhD Thesis* Technische Universität Ilmenau

[38] Yokoyama K, Oka T, Okada H, Fujine Y, Chiba A and Noto K 2003 Solid-liquid magnetic separation using bulk superconducting magnets *IEEE Trans. Appl. Supercond.* **13** 1592–5

[39] Yokoyama K, Oka T and Noto K 2009 A strong magnetic field generation by superconducting bulk magnets with the same pole arrangement *IEEE Trans. Appl. Supercond.* **19** 2178–81

[40] Oka T, Hirayama E, Kanai T, Ogawa J, Fukui S, Sato T, Yokoyama K and Nakamura T 2014 Strong magnetic field generator containing HTS bulk magnets and compact refrigerators *IEEE Trans. Appl. Supercond.* **24** 4900204

[41] Krabbes G, Fuchs G and Canders W R 2006 *High Temperature Superconductor Bulk Materials: Fundamentals, Processing, Properties Control, Application Aspects* (New York: Wiley)

[42] Ainslie M D and Fujishiro H 2015 Modelling of bulk superconductor magnetization *Supercond. Sci. Technol.* **28** 053002

[43] Ainslie M D, Srpcic J, Zhou D, Fujishiro H, Takahashi K, Cardwell D A and Durrell J H 2018 Toward optimization of multi-pulse, pulsed field magnetization of bulk high-temperature superconductors *IEEE Trans. Appl. Supercond.* **28** 6800207

[44] Bean C P 1964 Magnetization of high-field superconductors *Rev. Mod. Phys.* **36** 31–9

[45] Yan N, Kühnel M, Vasilyan S and Fröhlich T 2017 Calibration of the torsion force measurement system for the Lorentz force velocimetry application *2017 59th Ilmenau Scientific Coll. (11–15 September 2017)*

[46] Yan N, Kühnel M, Vasilyan S and Fröhlich T 2018 Torsion balance based system for high-precision force measurement in horizontal plane: I. Development concept *Meas. Sci. Technol.* accepted manuscript (https://doi.org/10.1088/1361-6501/aaba1f)

[47] Halbedel B, Vakaliuk O, Fröhlich T and Yan N 2017 Vorrichtung zur Ermittlung von Parametern einer elektrisch leitfähigen Substanz und dazugehöriges Verfahren, DE 10 2017 005 210.7 *German Patent* registered